(Received 10 March 2025, Accepted 29 April 2025, Scheduled 22 June 2025)

Microwave Scattering from Sea Surfaces: CBFM Hybridized to Kirchhoff and Weak-Coupling Approximations and to Identical Block PBFs

Christophe Bourlier*

IETR (Institut d'Electronique et des Technologies numéRiques) Laboratory
UMR CNRS 6164, Nantes Université, polytech Nantes, La Chantrerie, Nantes, France

ABSTRACT: In this paper, the characteristic basis function method (CBFM) is accelerated to calculate the monostatic and bistatic normalized radar cross sections from one-dimensional highly-conducting sea surfaces in the microwave bands (C and Ku). In the framework of the two-scale asymptotic model, the subsurface length of the block is judiciously derived to contain all the surface curvature components (small scale), and the associated PBFs, assumed to be identical for all blocks, are rapidly calculated from the Kirchhoff approximation. In addition, the reduced matrix calculation is accelerated by neglecting the interactions between far blocks and by introducing a roughness slight approximation (matrix-matrix products can be done from fast Fourier transforms), which also allows us to expedite the resolution of the linear system since the matrix is sparse. Numerical results show the efficiency of CBFM-KA.

1. INTRODUCTION

The scattering from rough sea surfaces in the microwave band has been a subject of great interest for several decades. The applications concern many areas such as remote sensing, radar surveillance, optics, and ocean acoustics. The calculation of normalized radar cross section (NRCS) can be divided into two categories. First, asymptotic models [1–5], where simplifying physical assumptions are introduced to obtain a closed-form expression of the scattered far field. The NRCS is obtained by deriving the second-order statistical moment. Second, full wave methods, like the well-known method of moments (MoM), [6–8] are applied to solve the boundary integral equations. However, the solution of the resulting linear system through a direct lower upper (LU) decomposition is usually limited by $\mathcal{O}(N^3)$ and $\mathcal{O}(N^2)$ complexities in CPU time and memory requirement, respectively, where N is the number of unknowns. This is computationally very expensive for an electrically-large multi-scale scatterer (i.e., many unknowns), like the sea surface. To overcome this issue, the stationary iterative forward-backward (FB) method [9] combined with the spectral acceleration (SA) [5, 10] is very efficient for the scattering from highly-conducting rough sea surfaces.

Compared with iterative solvers, direct solvers have some attractive features. For example, they do not suffer from unpredictable convergence and can efficiently solve the problems with multiple incidence angles (monostatic case). However, conventional direct solvers like LU are very expensive for large targets. To overcome this issue, efficient algorithms, based on subdivision of the entire geometry into several subdomains (blocks), have been developed to rigorously solve large problems. By this way, the solution is calculated from an iterative scheme, in which smaller size problems are solved from direct or iterative solvers. In this paper, one focuses on the characteristics basis function method (CBFM) [11]. It has shown its efficiency for the scattering from two- [12, 13] and three- [14–16] dimensional problems.

The CBFM principle splits up the surface into subsurfaces or blocks of smaller size, each of them being solved separately by calculating the primary basis functions (PBFs). Next, the coupling between them is accounted for via the computation of the reduced matrix, which involves the coupling matrices between the blocks. The third and last stage solves the linear system of smaller size N_R than that obtained from the MoM impedance matrix. Thus, for moderate N_R, LU can be applied.

To derive the NRCS, the well-known two-scale asymptotic model [17] can be applied. It results in that the NRCS is obtained from the modulation (a convolution product) of the small scale (given by the small perturbation method as a function of the sea curvature spectrum) by the large scale (given by the geometrical optics). The first novelty of this paper is to reproduce this statement from the CBFM. From CBFM, the contribution of the small scale can be represented by the PBFs. The size N_i or the associated small-scale block length L_{Small} of a given block i is determined so that all the components of the sea curvature spectrum are accounted for. Typically, we find that L_{Small} is of the order of one meter. In addition, to accelerate the PBFs calculation, the Kirchoff approximation (KA) [13] of complexity $\mathcal{O}(N_i)$ (instead of $\mathcal{O}(N_i^3)$ from LU) is applied. By construction, the PBFs are invariant by translation and rotation. If the block curvature statistics is entirely included, the

* Corresponding author: Christophe Bourlier (christophe.bourlier@univnantes.fr).

PBFs can be assumed identical for all blocks, which still decreases the computing time. For a Gaussian autocorrelation function (single-scale surface), this idea has been succinctly tested in [18]. The second novelty of this paper assumes that the coupling between the blocks (interaction of the small scale with the large scale) is weak, which expedites the calculation of the reduced matrix and also the resolution of the linear system, since the reduced matrix becomes sparse. In addition, to accelerate the matrix-matrix products, the roughness slight approximation is applied, which is based on the BMIA-CAG [5, 19–21] scheme.

The paper is organized as follows. Section 2 briefly addresses the CBFM and introduces the three assumptions to calculate the PBFs and the reduced matrix. Section 3 presents the monostatic and bistatic NRCS, and the last section gives concluding remarks.

2. CBFM COMBINED WITH APPROXIMATIONS

The electromagnetic problem to solve is depicted in Fig. 1. An incident wave of incidence angle $\theta_{\text{inc}} \in [0;\pi/2]$ illuminates a rough sea surface of profile $\zeta(x)$ defined in the Cartesian system (x,z). The scattered far field is measured in the direction $\theta_{\text{sca}} \in [-\pi/2;\pi/2]$. The purpose of the section is to calculate this field from the well-known method of moments (MoM) accelerated by the CBFM and introducing physical assumptions.

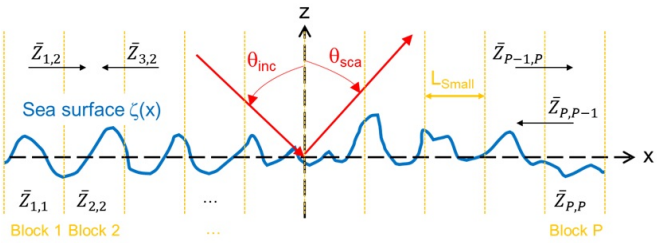

FIGURE 1. Geometry of the problem.

2.1. CBFM

Table 1 lists the inputs and outputs of CBFM. The use of the MoM leads to the linear system $\bar{\mathbf{Z}}\mathbf{X} = \mathbf{b}$, in which $\bar{\mathbf{Z}}$ is the impedance matrix, $\mathbf{b}$ a vector related to the incident field, and $\mathbf{X}$ the surface currents. For an highly-conducting surface and a point-matching MoM with pulse basis functions, the elements of $\bar{\mathbf{Z}}$ can be found in [8]. The scattered far field is computed from the currents $\mathbf{X}$ radiation.

The first stage of CBFM [11] decomposes the geometry into P sub-geometries (blocks). The impedance matrix $\bar{\mathbf{Z}}$ takes the form

$$\begin{bmatrix} \bar{\mathbf{Z}}_{1,1} & \bar{\mathbf{Z}}_{1,2} & \dots & \bar{\mathbf{Z}}_{1,P} \\ \bar{\mathbf{Z}}_{2,1} & \bar{\mathbf{Z}}_{2,2} & \dots & \bar{\mathbf{Z}}_{2,P} \\ \vdots & \vdots & \ddots & \vdots \\ \bar{\mathbf{Z}}_{P,1} & \bar{\mathbf{Z}}_{P,2} & \dots & \bar{\mathbf{Z}}_{P,P} \end{bmatrix} \begin{bmatrix} \mathbf{a}_1 \\ \mathbf{a}_2 \\ \vdots \\ \mathbf{a}_P \end{bmatrix} = \begin{bmatrix} \mathbf{b}_1 \\ \mathbf{b}_2 \\ \vdots \\ \mathbf{b}_P \end{bmatrix}, \quad (1)$$

where $\bar{\mathbf{Z}}_{p,p}$ is the self-impedance matrix of the block number p (see Fig. 1) and $\bar{\mathbf{Z}}_{p_1,p_2}$ the coupling-impedance matrix between

TABLE 1. Inputs ans outputs of CBFM.

Name	Definition
N	Total number of unknowns (input)
n_{OL}	Adjacent sample number (input)
P	Number of blocks (input)
$n_{\text{IPW}} \geq 1$	Integer defined in Eq. (3) (input)
$\epsilon_{\text{CBFM,SVD}}$	CBFM threshold of the SVD (input)
$P_0 \in [0;P]$	Adjacent block number (input)
$N_i = N/P$	Unknowns number of a block i
$N_{i'}$	Unknowns number of a block i with overlapping
$N_{\text{IPW},i}$	CBFM plane wave number of a block i (Eq. (3))
$N_{\text{IPW,SVD},i}$	CBFM plane wave number of a block i after SVD
$\bar{N}$	Mean value of N_i over $i \in [1;P]$
$\bar{N}_{\text{IPW}}$	Mean value of $N_{\text{IPW},i}$ over $i \in [1;P]$
$\bar{N}_{\text{IPW,SVD}}$	Mean value of $N_{\text{IPW,SVD},i}$ over $i \in [1;P]$

blocks p_1 and p_2. $\mathbf{a}_p$ and $\mathbf{b}_p$ are sub-vectors of the block p. Next, the primary basis function (PBF), $\mathbf{Y}_{i',k_{\text{IPW}}}$, is computed for each block by solving the linear system

$$\bar{\mathbf{Z}}_{i',i'}\mathbf{Y}_{i',k_{\text{IPW}}} = \mathbf{B}_{i',k_{\text{IPW}}}, \quad (2)$$

where $\bar{\mathbf{Z}}_{i,i}$ is the self-impedance matrix of block i, and the subscript prime indicates that block i is enlarged of n_{OL} $(=1)$ adjacent samples. The integer k_{IPW} stands for the k_{IPW}th plane wave (ranging from 1 to $N_{\text{IPW},i}$). The original version of CBFM [11] used $\mathbf{B}_{i',k_{\text{IPW}}} = \mathbf{b}_{i'}$ (single incident wave, $k_{\text{IPW}} = 1$), and secondary basis functions (SBFs) were calculated. In 2008 [22], a more efficient way was proposed to calculate the PBFs, and the computation of SBFs was not required. Lucente et al. [22] solved the linear system (2) from a collection of $N_{\text{IPW},i}$ incident waves $\{\mathbf{B}_{i',k_{\text{IPW}}}\}$, and the resulting vectors $\{\mathbf{Y}_{i',k_{\text{IPW}}}\}$ are stored in a matrix $\bar{\mathbf{J}}_i$ of size $N_i \times N_{\text{IPW},i}$. This means that the overlapped unknowns of $\mathbf{Y}_{i',k_{\text{IPW}}}$ are removed. The choice of $N_{\text{IPW},i}$ must be relevant to avoid that the size of the matrix is too big. The incident waves (vectors $\{\mathbf{B}_{i',k_{\text{IPW}}}\}$ in Eq. (2)) are assumed to be plane, and their incidence angles range from $-\pi/2$ to $\pi/2$. In addition, they are spaced equally, and in [13]

$$N_{\text{IPW},i} = \left\lfloor (k_0 L_i + 1)/n_{\text{IPW}} \right\rfloor, \quad (3)$$

where the symbol $\lfloor$ stands for the upper integer part, L_i the block length, and $k_0 = 2\pi/\lambda_0$ the wavenumber in vacuum. Since for a rough surface, $N_{\text{IPW},i}$ is overestimated, the number $n_{\text{IPW}} > 1$ is introduced (equal 2 for the simulations).

The redundant information due to the overestimation of $N_{\text{IPW},i}$ is eliminated via the use of a truncated singular value decomposition (SVD). This means that from a given threshold $\epsilon_{\text{CBFM,SVD}}$, the values for which the modulii of the normalized eigenvalues are smaller than $\epsilon_{\text{CBFM,SVD}}$ (equal 10^{-2} or 10^{-3}) are removed. The size of $\bar{\mathbf{J}}_\mathbf{i}$ becomes $N_i \times N_{\text{IPW,SVD},i}$, with $N_{\text{IPW,SVD},i} < N_{\text{IPW},i} < N_i$.

The second stage of CBFM consists in building a reduced linear system $\bar{\mathbf{Z}}^{\mathrm{R}}\mathbf{a}^{\mathrm{R}} = \mathbf{b}^{\mathrm{R}}$ defined as

$$\begin{bmatrix} \bar{\mathbf{Z}}^{\mathrm{R}}_{1,1} & \bar{\mathbf{Z}}^{\mathrm{R}}_{1,2} & \dots & \bar{\mathbf{Z}}^{\mathrm{R}}_{1,P} \\ \bar{\mathbf{Z}}^{\mathrm{R}}_{2,1} & \bar{\mathbf{Z}}^{\mathrm{R}}_{2,2} & \dots & \bar{\mathbf{Z}}^{\mathrm{R}}_{2,P} \\ \vdots & \vdots & \ddots & \vdots \\ \bar{\mathbf{Z}}^{\mathrm{R}}_{P,1} & \bar{\mathbf{Z}}^{\mathrm{R}}_{P,2} & \dots & \bar{\mathbf{Z}}^{\mathrm{R}}_{P,P} \end{bmatrix} \begin{bmatrix} \mathbf{a}^{\mathrm{R}}_1 \\ \mathbf{a}^{\mathrm{R}}_2 \\ \vdots \\ \mathbf{a}^{\mathrm{R}}_P \end{bmatrix} = \begin{bmatrix} \mathbf{b}^{\mathrm{R}}_1 \\ \mathbf{b}^{\mathrm{R}}_2 \\ \vdots \\ \mathbf{b}^{\mathrm{R}}_P \end{bmatrix}, \quad (4)$$

where the submatrix $\bar{\mathbf{Z}}^{\mathrm{R}}_{i,j}$ and subvector $\mathbf{b}^{\mathrm{R}}_i$ are defined as

$$\begin{cases} \bar{\mathbf{Z}}^{\mathrm{R}}_{i,j} = \bar{\mathbf{J}}^{\mathrm{H}}_i \bar{\mathbf{Z}}_{i,j} \bar{\mathbf{J}}_j & [N_{\mathrm{IPW,SVD},i} \times N_{\mathrm{IPW,SVD},j}] \\ \mathbf{b}^{\mathrm{R}}_j = \bar{\mathbf{J}}^{\mathrm{H}}_j \mathbf{b}_j & [N_{\mathrm{IPW,SVD},i} \times 1] \end{cases}. \quad (5)$$

Moreover, the symbol H stands for the conjugate transpose operator, and the indexes i and j range from 1 to P.

The last step of CBFM solves the reduced linear system $\bar{\mathbf{Z}}^{\mathrm{R}}\mathbf{a}^{\mathrm{R}} = \mathbf{b}^{\mathrm{R}}$. The unknown vector $\mathbf{X}_i$ of the block i equals $\mathbf{X}_i = \bar{\mathbf{J}}_i \mathbf{a}^R_i$.

The problem is then represented by the square reduced matrix of size $N^2_R = (P\bar{N}_{\mathrm{IPW,SVD}})^2$ instead of a square matrix of size $N^2 = (P\bar{N})^2$. Then, the reduction factor is $\beta^2 = (\bar{N}/\bar{N}_{\mathrm{IPW,SVD}})^2$. If multiple excitations $\{\mathbf{b}\}$ (for instance, monostatic case) are considered, then the storing of $\bar{\mathbf{Z}}^{\mathrm{R}}$ avoids to apply iterative solvers (like FBSA or conjugate gradient), and the surface currents are rapidly calculated.

2.2. Complexity

Theoretically, the CBFM complexity is

$$C_{\mathrm{CBFM}} = \sum_{i=1}^{i=3} C_i = \sum_{i=1}^{i=3} \alpha_i C'_i \text{ where } \alpha_3 \approx \alpha_2^2, \quad (6)$$

and C'_i stands for the complexity of the ith conventional CBFM stage expressed as

$$\begin{aligned} &C'_1 = 2P\bar{N}_{\mathrm{IPW}}\mathcal{O}(\bar{N}^3), \quad C'_2 = 2P^2\bar{N}_{\mathrm{IPW,SVD}}\mathcal{O}(\bar{N}^2) \\ &C'_3 = \mathcal{O}(\bar{N}^3_R), \end{aligned} \quad (7)$$

where $N_R = \bar{N}_{\mathrm{IPW,SVD}}P$ is the reduced matrix size, and α_2 is defined by Eq. (8). In C'_1, the factor two comes from LU plus SVD.

2.3. Approximations

For a collection of N_{IPW} waves, the PBFs calculation requires to solve the linear system PN_{IPW} times, leading to a complexity of $2P\bar{N}_{\mathrm{IPW}}\mathcal{O}(N_i^3)$ ($N_{i'} \approx N_i$) from the direct solver LU plus SVD. To reduce the complexity of this operation to $P\bar{N}_{\mathrm{IPW}}\mathcal{O}(N_i^3)$ ($\alpha_1 = 1/2$ in Eq. (6)), the Kirchoff approximation (KA) is applied. For a perfectly-conducting surface, this leads to $\mathbf{Y}_{i,k_{\mathrm{IPW}}} = 2\mathbf{B}_{i,k_{\mathrm{IPW}}}$. In the microwave band, both the real and imaginary parts of the sea complex relative permittivity is high, which allows us to apply the impedance boundary condition. This implies that the impedance matrix is the weighted sum of those obtained from the Dirichlet and Neumann boundary conditions [5]. We assume that $\mathbf{Y}_{i,k_{\mathrm{IPW}}} \approx 2\mathbf{B}_{i,k_{\mathrm{IPW}}}$ under the KA approximation. In [13], numerical simulations showed that this approximation predicts very good results. It is important to underline that the PBFs are not the final solution: they can be interpreted as merely macro-basis functions. This, in turn, enables us to calculate them with a good approximation, without compromising the accuracy of the final solution.

In addition, as explained in the introduction, since the PBFs are invariant by rotation and translation, we assume that the PBFs of all the blocks are identical. This implies in Eq. (6) that $\alpha_1 = 1/P$ and $\alpha_1 = 1/(2P)$ if KA is applied.

Equation (4) shows that $M = P^2$ sub-matrices $\{\bar{\mathbf{Z}}^{\mathrm{R}}_{i,j}\}$ must be computed. It is important to underline that the reduced submatrix $\bar{\mathbf{Z}}^{\mathrm{R}}_{p_1,p_2}$ characterizes the coupling between the blocks p_1 and p_2. For far blocks, we can expect that this coupling should be negligible. To account for this phenomenon, only matrices $\{\bar{\mathbf{Z}}^{\mathrm{R}}_{i\in[1;P],J}\}$ are calculated, where $J \in [j_{\min}; j_{\max}]$, $j_{\min} = \max(1, i - P_0)$, and $j_{\max} = \min(P, P_0 + i)$, and $P_0 \in [0; P-1]$ is the number of adjacent blocks. The submatrix number is $M_0 = P_0(2P - P_0 - 1) + P$ (we can check that for $P_0 = P - 1$, $M_0 = M^2$), and the complexity of the matrix-matrix products (computation of $\{\bar{\mathbf{Z}}^{\mathrm{R}}_{i,j}\}$) is multiplied by the factor $\alpha_2 = M_0/M \in]0; 1]$ which equals

$$\alpha_2 = \frac{P_0(2P - P_0 - 1) + P}{P^2} \approx \frac{2P_0 + 1}{P} \text{ for } 0 \leq P_0 \ll P. \quad (8)$$

In addition, the reduced matrix becomes sparse, and the LU decomposition is accelerated by a factor $\alpha_3 \approx \alpha_2^2$.

To further accelerate the matrix-matrix product $\bar{\mathbf{Z}}_{i,j}\bar{\mathbf{J}}_j$, a roughness slight approximation is applied, which allows us to express the sub-matrix $\bar{\mathbf{Z}}_{i,j}$ as a sum of Toeplitz matrices, as shown in the appendix. This implies that the matrix-matrix product $\bar{\mathbf{Z}}_{i,j}\bar{\mathbf{J}}_j$ can be done from fast Fourier transforms (FFT).

3. NUMERICAL RESULTS

3.1. Determination of the Block Length L_{Small}

The size N_j or the associated small-scale surface length L_{Small} of a given block j is determined so that all the components of the sea *curvature* spectrum are accounted for to reproduce the two-scale model. To evaluate L_{Small}, the following criterion is defined

$$w_i(x) = \frac{\sigma_i(x)}{\sigma_i(\infty)}, \quad \sigma_i^2(x) = \int_{\frac{2\pi}{x}}^{\infty} k^i S(k) dk, \quad (9)$$

where $S(k)$ is the sea surface isotropic height spectrum. Moreover, $\sigma_i^2(x)$ is the cumulative (because it depends on x) variance of the surface height, i.e., $i = 0$, slope, i.e., $i = 2$, and curvature, i.e., $i = 3$. If the surface length x is infinity, then the variance equal to $\sigma_i^2(\infty)$ is obtained and $w_i(x) = 1$. In other words, all the roughness scales are included.

Figure 2 plots w versus the surface length for a wind speed $u_{10} = 5$ m/s (defined at ten meters above the sea mean level). The Elfouhaily et al. spectrum [24], S, is used. As the surface length increases, w increases to tend to 1, and this limit is reached faster as i grows. Choosing a threshold of 0.995,

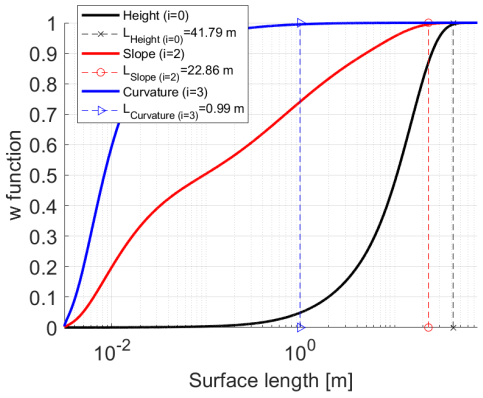

FIGURE 2. w versus the surface length. $u_{10} = 5\,\text{m/s}$.

the length $L_{\text{Small},i}$ is defined as $w_i(L_{\text{Small},i}) = 0.995$ and can be physically interpreted as a correlation length reported in the legend. For $i = 3$, Fig. 3 shows that $L_{\text{Small},3} = L_{\text{Small}} = 1\,\text{m}$. In the following, $L_{\text{Small}} = 0.96\,\text{m}$.

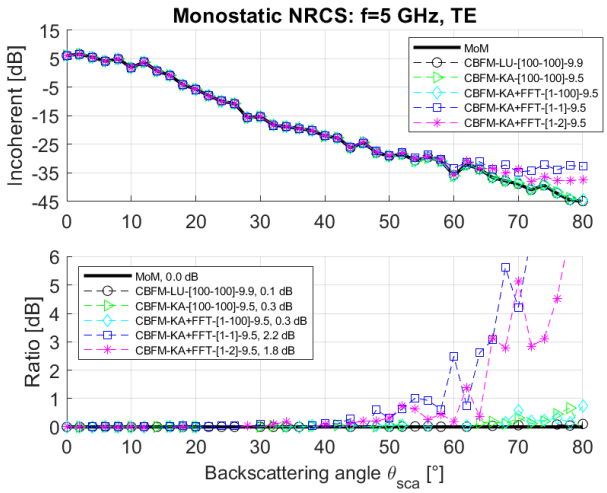

FIGURE 3. Top: Monostatic NRCS versus the incidence angle $\theta_{\text{sca}} = -\theta_{\text{inc}}$. Bottom: Ratio $\text{NRCS}/\text{NRCS}_{\text{MoM}}$ (becomes a difference) in dB scale. $f = 5$ GHz, $u_{10} = 5$ m/s, $L = 96$ m, $N_r = 20$, $N = 12,800$, $P = 100$, $n_{\text{OL}} = 1$, $\kappa_0 = 0.2$, $\epsilon_0 = 0.1$ and the polarization is TE. In addition, for LU, $\epsilon_{\text{CBFM,SVD}} = 10^{-2}$, whereas for KA, $\epsilon_{\text{CBFM,SVD}} = 10^{-3}$.

For the height, $L_{\text{Small},0} \approx 41.8\,\text{m}$. The wave number of the most energetic wave is defined as $k_p = g\Omega^2/u_{10}^2$, where $g = 9.81\,\text{m}\cdot\text{s}^{-2}$ and $\Omega = 0.84$. For $u_{10} = 5\,\text{m/s}$, the spatial period $L_p = 2\pi/k_p \approx 22.7\,\text{m} < L_{\text{Small},0}$ because sea waves of lesser energy and also of smaller wave numbers (or larger spatial periods) contribute as well. This means that the surface length L must exceed $L_{\text{Small},0}$ to include all the surface heights. In the following, $L = 96\,\text{m}$.

3.2. Normalized Radar Cross Section

If the surface has a finite extent, edge diffraction can occur because the incident field does not vanish on the edges of the surface. To reduce this phenomenon, a Gaussian tapered incident wave is used instead of a plane wave. The Thorsos wave is defined as [8, 24] (of magnitude one)

$$\psi_{\text{inc}}(\mathbf{r}) = \underbrace{e^{j\mathbf{k}_{\text{inc}}\cdot\mathbf{r}}}_{\text{Plane wave}}\ \underbrace{e^{-\frac{(x+z\tan\theta_{\text{inc}})^2}{g^2}}}_{\text{Damping factor}}\ \underbrace{e^{jw(\mathbf{r})\mathbf{k}_{\text{inc}}\cdot\mathbf{r}}}_{\text{Corrective term}} \tag{10}$$

where

$$w(\mathbf{r}) = \left[\frac{2(x+z\tan\theta_{\text{inc}})^2}{g^2} - 1\right]\frac{1}{(k_0 g\cos\theta_{\text{inc}})^2}, \tag{11}$$

and $\mathbf{k}_{\text{inc}} = k_0(\sin\theta_i\hat{\mathbf{x}} - \cos\theta_i\hat{\mathbf{z}})$ the incident direction. At the far distance r', the normalized radar cross section (NRCS, dimensionless) is defined as

$$\text{NRCS} = \lim_{r'\to\infty}\frac{r'}{2\eta_0}\frac{|\psi_{\text{sca}}^{\infty}|^2}{p_{\text{inc}}}, \tag{12}$$

where η_0 is the vacuum wave impedance, p_{inc} the incident power defined on the rough surface mean plane $z = 0$ (Eq. (1.34) of [8] and behaves as $1/\eta_0$), and $\psi_{\text{sca}}^{\infty}$ (behaves as $1/\sqrt{r'}$) the scattered far field. It is calculated by radiating the surface currents using the Huygens principle. It is important to underline that the Thorsos's wave is not valid at grazing incidence angles. The sea surface is generated from the well-known spectral method [5] (Section 1.6) and obeys the Elfouhaily et al. spectrum [23], and the sampling step is eight points per wavelength λ_0.

For the TE polarization, Fig. 3 plots the monostatic NRCS versus the incidence angle $\theta_{\text{sca}} = -\theta_{\text{inc}}$ and Fig. 4 the bistatic one for $\theta_{\text{inc}} = 30°$. Figs. 5 and 6 plot the same variations, but for the TM polarization. At the bottom, to better highlight the differences, the ratio $\text{NRCS}/\text{NRCS}_{\text{MoM}}$ is plotted in dB scale ($10|\log_{10}(\text{NRCS}/\text{NRCS}_{\text{MoM}})|$). The frequency $f = 5\,\text{GHz}$ and the complex relative permittivity $\epsilon_r = 69.2 + 35.7j$.

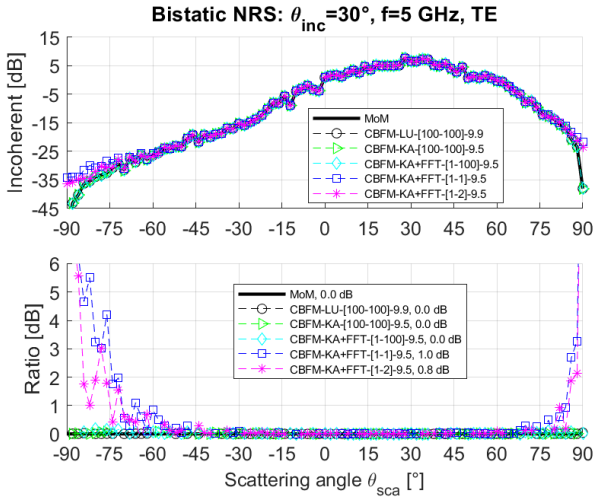

FIGURE 4. Bistatic NRCS versus the scattering angle θ_{sca}. Same parameters as in Fig. 3 and $\theta_{\text{inc}} = 30°$.

In the legend, "MoM" corresponds to the brute force MoM, and "CBFM-Method" labels CBFM, where "Method" is either "LU" or "KA" for the PBFs computation. In addition, "+FFT"

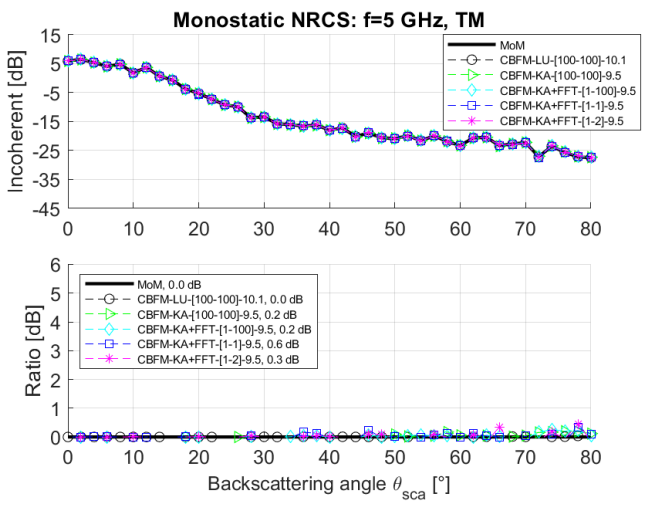

FIGURE 5. Same variations as in Fig. 3 but for the TM polarization.

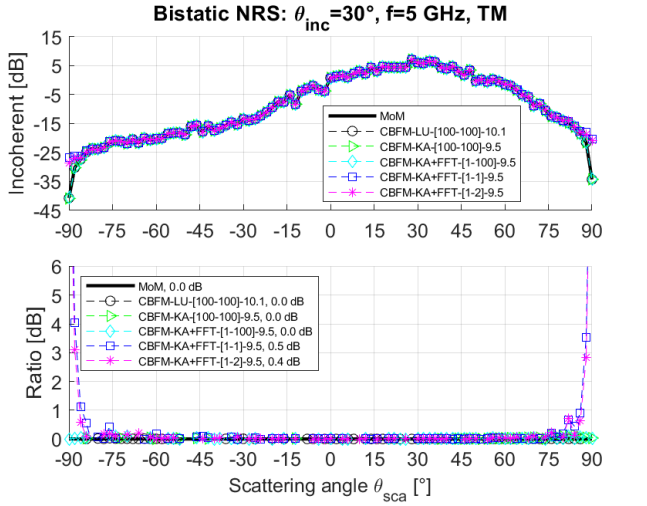

FIGURE 6. Same variations as in Fig. 4 but for the TM polarization.

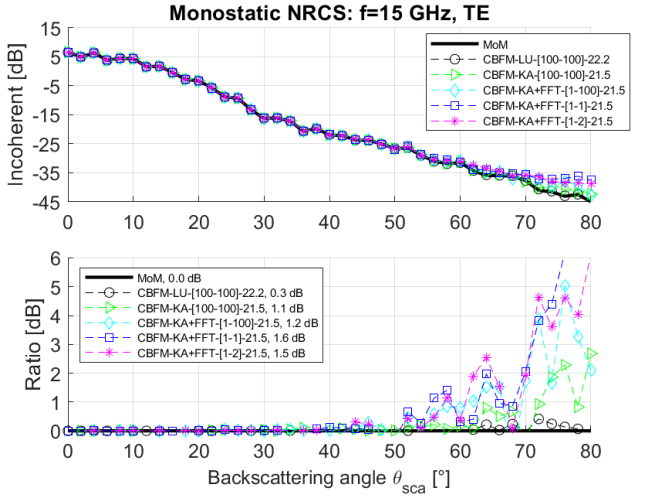

FIGURE 7. Same variations as in Fig. 3, but $f = 15\,\text{GHz}$ and $N = 52,800$.

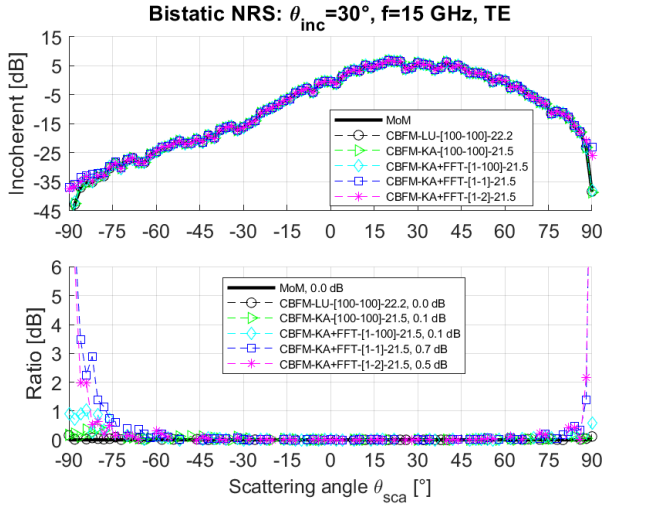

FIGURE 8. Same variations as in Fig. 4, but $f = 15\,\text{GHz}$.

means that the acceleration presented in the appendix is applied, where $\kappa_0 = 0.2$ and $\epsilon_0 = 0.1$ in Eqs. (A8) and (A9). The three numbers $[n_{\text{PBF}}, P_0] - (N/N_R)^2 = \beta^2$ are also reported in the legend, where N is the size of the impedance matrix $\bar{\mathbf{Z}}$, N_R that of the reduced matrix $\bar{\mathbf{Z}}^{\text{R}}$, and n_{PBF} the number of times that the PBFs are calculated. $n_{\text{PBF}} = 1$ implies that the PBFs are assumed to be identical for all blocks and are calculated only once.

For the ratio, the additional number in the legend is the ratio mean value over $\theta_{\text{sca}} \in [0, 80°]$ or $\theta_{\text{sca}} \in [-90, 90]°$ (bistatic case). The NRCS is computed from $N_r = 20$ number of surface realizations.

As we can see in Figs. 3, 4, 5, and 6, CBFM-LU matches well with the MoM reference solution, and when the acceleration is applied with $n_{\text{PBF}} = 1$, the precision remains good. This means that the number of blocks $P = 100$ is well chosen and that $\kappa_0 = 0.2$, $\epsilon_0 = 0.1$ is a good choice. In Eq. (A1), for $P_0 = P = 100$, the mean (over N_r and block pairs equal to 9326 that satisfy Eqs. (A8) and (A9)) convergence order $\bar{Q} \approx 2.26$, meaning that the acceleration converges rapidly.

As P_0 increases, the agreement between CBFM-KA+FFT and the MoM is slightly improved for grazing angles. As expected, for $|\theta_{\text{sca}}|$ approaching 90 degrees, more far interaction blocks (P_0 increases) are needed, and this feature is more important for the TE polarization. In Fig. 5, CBFM-KA+FFT-[1, 1] matches very well with the MoM.

Figures 3, 4, 5, and 6 also reveal that the CBFM reduces the size of the initial MoM linear system to a factor $\beta^2 = (N_R/N)^2 \approx 9.5$ ($N = 12,800$). It is nearly constant versus the polarization and the method KA or LU. It is important to point out that the threshold $\epsilon_{\text{CBFM,SVD}}$ of KA equals 10^{-3}, instead of 10^{-2} for LU, to obtain a similar $\bar{N}_{\text{IPW,SVD}}$ for both methods and thus, the same precision.

Figures 7, 8, 9, and 10 plot the same variations as in Figs. 3, 4, 5, and 6, but the frequency $f = 15\,\text{GHz}$ (wind speed $u_{10} = 5\,\text{m/s}$ and surface length $L = 96\,\text{m}$). The number of unknowns $N = 51,200$ and the complex relative permittivity $\epsilon_r = 37.6 + 39.8j$. As we can see, for the TE polarization, CBFM-LU matches well with the MoM reference solution, and when the acceleration is applied with $n_{\text{PBF}} = 1$, the precision

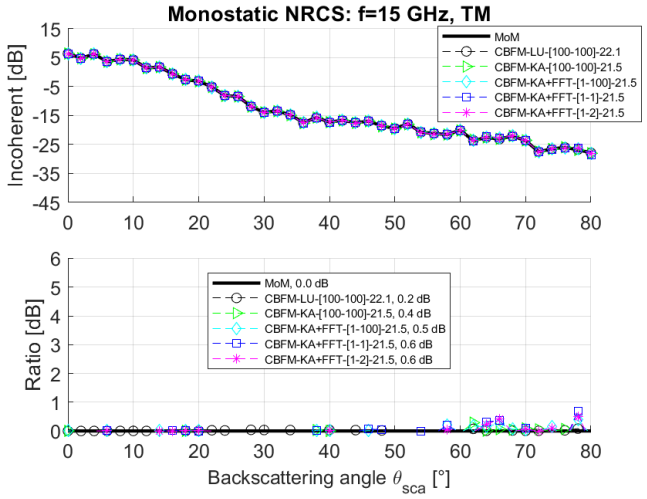

FIGURE 9. Same variations as in Fig. 5, but $f = 15\,\text{GHz}$.

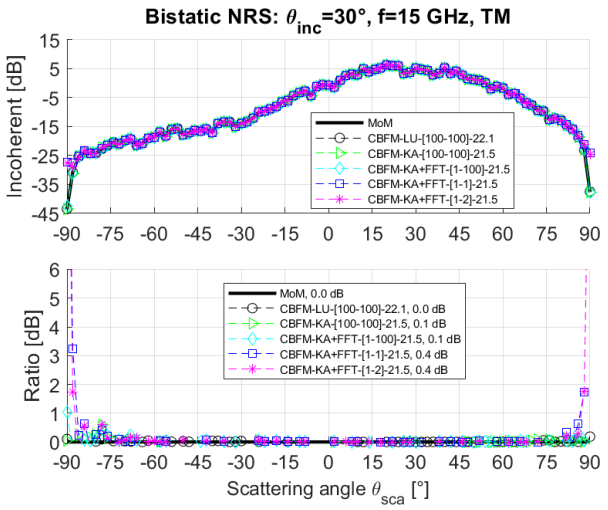

FIGURE 10. Same variations as in Fig. 5, but $f = 15\,\text{GHz}$.

remains satisfactory. This implies that the number of blocks is not sensitive to the frequency. For grazing angles, more far interactions blocks P_0 are needed to decrease the difference with the MoM. For the TM polarization, all the methods predict good results. The reducetion factor $\beta^2 \approx 21.5$, which shows that the CBFM is more efficient as the frequency increases since for $f = 5\,\text{GHz}$, $\beta^2 \approx 9.5$. In addition, the mean convergence order $\bar{Q} \approx 2.52 > 2.26$ obtained for $f = 5\,\text{GHz}$, which slightly increases as f grows.

All these results are consistent with the TSM (two-scale model), one of the first-published scattering asymptotic methods to calculate the monostatic sea NRCS. The PBFs of each block are related to the contribution of the small scale. From TSM, the PBFs are obtained from SPM1 (first-order small perturbation method), related to the surface curvature spectrum. That is why the block length is chosen such that all the surface curvature roughnesses are accounted for. The characteristic matrix allows the surface currents to interact between the blocks, which is similar to modulate the small scale by the large scale. The TSM is based on this statement. The fact that CBFM with $n_{\text{PBF}} = 1$ predicts good results implies that the multiple interactions between the blocks are negligible, and only two adjacent blocks significantly interact. This again is consistent with the TSM, since the large scale contribution is determined from the first-order geometric optics approximation, in which the multiple reflections are omitted, like SPM. It is also well known that the TSM predicts better results for the TM case than the TE one.

From Eq. (6), the CBFM CPU time is defined as $t_{\text{CBFM}} = t_1 + t_2 + t_3$, where t_i stands for the ith-CBFM stage time. The computer machine is Intel(R) Xeon(R) Gold 6142 CPU @ 2.60 GHz (4 processors, 32 cores) with 512 GB. The time allocated to fill the MoM impedance matrix $t_{\text{Fill}} \approx 1968\,\text{s}$ or impedance sub-matrices is not accounted for. The function linsolve of MatLab, based on LU algorithm, is applied. For multiple excitations (41), no loop is needed, and this function is very efficient because it is parallelized (on the 32 cores).

The CPU time of the brute force MoM is $t_{\text{MoM}} \approx 2223\,\text{s}$. For CBFM-LU it equals 964 s, whose $t_2 \approx 940\,\text{s}$ are allocated to calculate the characteristic matrix. If the acceleration, based on FFT, is applied, $t_2 \approx 1444s$. Theoretically, $t_{2,\text{FFT}}/t_2 \approx 1/2 + 4\bar{Q}^2\bar{N}\log_2\bar{N}/\bar{N}^2 \approx 0.95$, where $\bar{N} = 512$. This is consistent with the numerical value, and $\bar{N}$ is not large enough to achieve a gain. If $P_0 = 1$, then $t_{2,\text{FFT}} = t_2 \approx 31\,\text{s}$. Theoretically, the ratio time $t_2/t_{2,P_0=1} = 1/\alpha_2 = P/(2P_0+1) = 100/3 \approx 33$. Numerically, $1/\alpha_2 = 940/31 \approx 30$, which is in agreement with the theoretical value. The total time is about 39 s, which leads to a gain in saving time of $2223/39 \approx 57$ in comparison to the brute force MoM. For $P_0 = 2$, this ratio is about 31.

The CBFM hybridized with KA, and for $n_{\text{PBF}} = 1$, the time $t_1 = 0.16\,\text{s}$, whereas for $n_{\text{PBF}} = 100$ and with LU, $t_1 = 16.39\,\text{s}$. The gain in saving time is $16.39/0.16 \approx 104$, and the theoretical value $1/\alpha_1 = 2P = 200$. This means that the major time is allocated to calculate the SVD.

4. CONCLUSION

In this paper, the CBFM is combined with three physical approximations to calculate the monostatic and bistatic microwave NRCSs from sea surfaces. Typically, the block lengths are equal to one meter, and only one adjacent block is accounted for the reduced matrix calculation, in which the matrix-matrix products are expedited by using FFTs. Moreover, the Kirchoff approximation is applied to compute the PBFs by considering perfectly-conducting subsurfaces, and PBFs are assumed to be identical for all blocks. The numerical results show that the precision of the hybridized method is only altered for grazing scattering angles, and for a number of unknowns $N = 52,800$ ($f = 15\,\text{GHz}$), the gain in saving time, in comparison to the brute force MoM, is of the order of 57. This gain is an order of magnitude and of course depends on the architecture of the computer machine. This gain should increase with N. So, a prospect of this paper is to extend the formulation to a two-dimensional sea surface since for the one-dimensional case the obtained results are very promising.

APPENDIX A. MATRIX-VECTOR PRODUCT ACCELERATION

The reduced matrix needs to calculate $2P^2$ matrix-vector products. For two far blocks, this appendix shows that the coupling matrix $\bar{\mathbf{Z}}_{i,j}$ can be expressed as a sum of Toeplitz matrices. For any vector $\mathbf{v}$, this implies that the matrix-vector product $\bar{\mathbf{Z}}_{i,j}\mathbf{v}$ (applied P^2 times if criterion (A8) is satisfied for any (i,j)) can be done from fast Fourier transforms. This way is analog to the Banded-Matrix-Iterative-Approach/CAnonical Grid (BMIA-CAG) [5, 19–21]. The main difference is that the current $\mathbf{r}_{j,n} = (x_{j,n}, z_{j,n})$ and observation $\mathbf{r}_{i,m} = (x_{i,m}, z_{i,m})$ points do not belong to the same surface.

For two given blocks (i,j) and from the Dirichlet boundary condition, the elements of the coupling matrix $\bar{\mathbf{Z}}_{i,j}$ depend on $f_{m,n} = \mathrm{H}_0^{(1)}(k_0\|\mathbf{r}_{i,m} - \mathbf{r}_{j,n}\|)$, where $\mathrm{H}_0^{(1)}$ is the zeroth order Hankel function of first kind and k_0 the wave number in free space. Introducing $x_d = |x_{i,m} - x_{j,n}| = |x_m - x_n|$ and $z_d = z_{i,m} - z_{j,n} = z_m - z_n$, the expansion of $f_{m,n}$ with respect to $u = x_d/z_d$ around zero leads from [5] to

$$f_{m,n} \approx \sum_{q=0}^{Q}\sum_{p=0}^{2q} C_{2q}^{p} z_m^{2q-p} a_q(x_d)\,(-z_n)^p\,, \tag{A1}$$

where

$$a_q(x_d) = \frac{\mathrm{H}_q^{(1)}\,(k_0 x_d)}{q!}\left(\frac{-k_0}{2x_d}\right)^q, \tag{A2}$$

and

$$C_{2q}^{p} = \frac{(2q)!}{p!(2q-p)!}. \tag{A3}$$

The coefficients $a_q(x_d)$, which depend one the abscissa difference $|x_m - x_n|$, can be expressed from $\mathrm{H}_0^{(1)}$ and $\mathrm{H}_1^{(1)}$ by using $\mathrm{H}_{q+1}^{(1)}(z) = \frac{2q}{z}\mathrm{H}_q^{(1)}(z) - \mathrm{H}_{q-1}^{(1)}(z)$ [25]. The matrix-vector product $\bar{\mathbf{Z}}_{i,j}\mathbf{v}$ can be expressed as [5]

$$\bar{\mathbf{Z}}_{i,j}\mathbf{v} = \sum_{q=0}^{Q}\sum_{p=0}^{2q} \bar{\mathbf{T}}_{q,p}^{\mathrm{post}}\left[\bar{\mathbf{T}}_{q}^{\mathrm{Toe}}\left(\bar{\mathbf{T}}_{q,p}^{\mathrm{pre}}\mathbf{v}\right)\right], \tag{A4}$$

where

$$\begin{cases} \bar{\mathbf{T}}_{q,p}^{\mathrm{pre}} \text{ a } \textit{diagonal} \text{ matrix of pre-multiplication of elements } \alpha_n\,(-z_n)^p \\ \bar{\mathbf{T}}_{q}^{\mathrm{Toe}} \text{ a } \textit{Toeplitz} \text{ matrix of elements } a_q(x_d) \\ \bar{\mathbf{T}}_{q,p}^{\mathrm{post}} \text{ a } \textit{diagonal} \text{ matrix of post-multiplication of elements } C_{2q}^{p} z_m^{2p-p} \end{cases}, \tag{A5}$$

and $\alpha_n = j|\Delta_n|\sqrt{1+\gamma_n}/4$, where Δ_n is the sampling step and γ_n the surface slope. Since $\bar{\mathbf{T}}_{q,p}^{\mathrm{pre}}$ and $\bar{\mathbf{T}}_{q,p}^{\mathrm{post}}$ are diagonal matrices, the complexities of the operations $\bar{\mathbf{T}}_{q,p}^{\mathrm{pre}}\mathbf{v}$ and $\bar{\mathbf{T}}_{q,p}^{\mathrm{post}}\mathbf{v}$ are $\mathcal{O}(N_i + N_j)$, where $\bar{\mathbf{Z}}_{i,j}$ is of size $N_i \times N_j$. In addition, since $\bar{\mathbf{T}}_{q}^{\mathrm{Toe}}$ is a Toeplitz matrix, the complexity of $\bar{\mathbf{T}}_{q}^{\mathrm{Toe}}\mathbf{v}$ is $\mathcal{O}(N\log N)$ where $N = N_i + N_j$. Then, the resulting complexity of $\bar{\mathbf{Z}}_{i,j}\mathbf{v}$ is of the order of

$$C = (Q+1)^2\,\mathcal{O}(N\log N + 2N) \approx Q^2\mathcal{O}(N\log N), \tag{A6}$$

for $(N,Q) \gg 1$.

For any Toeplitz matrix $\bar{\mathbf{A}} = \bar{\mathbf{Z}}_{i,j}$ of sizes $N_i \times N_j$ and for any vector $\mathbf{v}$ of sizes $N_j \times 1$, the component $u_{m\in[1;N_i]}$ of the vector $\mathbf{u} = \bar{\mathbf{A}}\mathbf{v}$ can be expressed as $u_m = \sum_{n=1}^{N_j} A_{m-n}v_n$, which is a convolution product done in the Fourier domain. This leads to

$$\mathbf{u} = \mathrm{IFFT}\left[\mathrm{FFT}\,(\mathbf{a})\,\mathrm{FFT}\,(\mathbf{w})\right]|_{i\in[1;N_i]}\,, \tag{A7}$$

where $\mathbf{a} = [A(x_{i,1} - x_{j,1})\ A(x_{i,2} - x_{j,1}) \ldots A(x_{i,N_i} - x_{j,1})\ \ A(x_{i,1} - x_{j,1})\ \ A(x_{i,1} - x_{i,N_j})\ \ A(x_{i,1} - x_{j,N_j-1}) \ldots A(x_{i,1} - x_{j,2})]$ and $\mathbf{w} = [\mathbf{v}^{\mathrm{T}}\ \mathbf{0}_{N_i\times 1}]$ are vectors of length $N_i + N_j = N$. In the above equation, the subscript $m \in [1;N_i]$ means that only the first N_i elements are kept since the resulting vector $\mathbf{u}$ has a length N_i. The element A is computed from Eq. (A2). The resulting complexity is $\mathcal{O}(N\log N)$ instead of $\mathcal{O}(N^2)$. In addition, $(Q+1)(N-1) \approx (Q+1)N$ elements of the matrix $\bar{\mathbf{A}}$ are computed instead of N_iN_j. In [5], the same way is addressed for the Neumann boundary condition, and Eq. (A4) can be applied if

$$\kappa_{i,j} = \frac{\lambda_0}{d_{i,j}}\frac{\sigma_{z_{i,j}}^2}{\lambda_0^2} < \kappa_0, \tag{A8}$$

and

$$Q = q+1 \text{ such as } \frac{\mathrm{norm}\,(F_{q+1} - F_q)}{\mathrm{norm}\,(F_{q+1})} \le \epsilon_0, \tag{A9}$$

where $d_{i,j} = |x_{i,0} - x_{j,0}|$, in which $x_{i,0}$ is the middle abscissa of the block i. In addition, $\sigma_{z_{i,j}} = \sqrt{\langle z_{i,j}^2\rangle}$, where $z_{i,j} = z_i - z_j$ is the height difference between z_i and z_j of the blocks i and j, respectively. Typically, $\kappa_0 \in [0.1; 0.2]$. In Eq. (A1), the sum over Q is stop, given $Q = q+1$, when the relative norm between two consecutive terms (F_{q+1}, F_q) is smaller than a threshold named ϵ_0. Typically, $\epsilon_0 = 0.1$.

Equation (A8) shows that this acceleration can be applied if $\lambda_0/d_{i,j} < 1$, meaning that the horizontal distance between two blocks is larger than the wavelength λ_0 and, $\sigma_{z_{i,j}}/\lambda_0 < 1$, meaning that the mean height difference between two blocks is smaller than λ_0.

REFERENCES

[1] Voronovich, A., "Small-slope approximation for electromagnetic wave scattering at a rough interface of two dielectric half-spaces," *Waves in Random Media*, Vol. 4, No. 3, 337, 1994.

[2] Elfouhaily, T. M. and C.-A. Guérin, "A critical survey of approximate scattering wave theories from random rough surfaces," *Waves in Random Media*, Vol. 14, No. 4, R1, 2004.

[3] Bourlier, C. and N. Pinel, "Numerical implementation of local unified models for backscattering from random rough sea surfaces," *Waves in Random and Complex Media*, Vol. 19, No. 3, 455–479, 2009.

[4] Pinel, N. and C. Boulier, *Electromagnetic Wave Scattering from Random Rough Surfaces: Asymptotic Models*, John Wiley & Sons, 2013.

[5] Bourlier, C., *Radar Propagation and Scattering in A Complex Maritime Environment: Modeling and Simulation from MatLab*, Elsevier, 2018.

[6] Harrington, R. F., *Field Computation by Moment Methods*, Macmillan, 1968.

[7] Tsang, L., J. A. Kong, K.-H. Ding, and C. O. Ao, *Scattering of Electromagnetic Waves: Numerical Simulations*, John Wiley & Sons, 2004.

[8] Bourlier, C., N. Pinel, and G. Kubické, *Method of Moments for 2D Scattering Problems: Basic Concepts and Applications*, John Wiley & Sons, 2013.

[9] Holliday, D., L. L. DeRaad, and G. J. St-Cyr, "Forward-backward: A new method for computing low-grazing angle scattering," *IEEE Transactions on Antennas and Propagation*, Vol. 44, No. 5, 722, 1996.

[10] Chou, H.-T. and J. T. Johnson, "A novel acceleration algorithm for the computation of scattering from rough surfaces with the forward-backward method," *Radio Science*, Vol. 33, No. 5, 1277–1287, 1998.

[11] Prakash, V. V. S. and R. Mittra, "Characteristic basis function method: A new technique for efficient solution of method of moments matrix equations," *Microwave and Optical Technology Letters*, Vol. 36, No. 2, 95–100, 2003.

[12] Yagbasan, A., C. A. Tunc, V. B. Erturk, A. Altintas, and R. Mittra, "Characteristic basis function method for solving electromagnetic scattering problems over rough terrain profiles," *IEEE Transactions on Antennas and Propagation*, Vol. 58, No. 5, 1579–1589, 2010.

[13] Bourlier, C., "Rough layer scattering filled by elliptical cylinders from the method of moments combined with the characteristic basis function method and the Kirchoff approximation," *Journal of the Optical Society of America A*, Vol. 38, No. 10, 1581–1593, 2021.

[14] Laviada, J., M. R. Pino, and F. Las-Heras, "Generation of excitation-independent characteristic basis functions for three-dimensional homogeneous dielectric bodies," *IEEE Transactions on Antennas and Propagation*, Vol. 59, No. 9, 3318–3327, 2011.

[15] Li, C. and R. Mittra, "Characteristic basis function method for fast analysis of 3-D scattering from objects buried under rough surfaces," *IEEE Transactions on Geoscience and Remote Sensing*, Vol. 57, No. 8, 5252–5265, 2019.

[16] Bourlier, C., "Characteristic Basic Function Method accelerated by a new Physical Optics approximation for the scattering from a dielectric object," *Progress In Electromagnetics Research B*, Vol. 103, 177–194, 2023.

[17] Wright, J., "A new model for sea clutter," *IEEE Transactions on Antennas and Propagation*, Vol. 16, No. 2, 217–223, Mar. 1968.

[18] Yuan, J. and H. Ye, "Modeling of EM scattering from 1D random rough surface with common characteristic basis function method," in *2020 IEEE MTT-S International Wireless Symposium (IWS)*, 1–3, Shanghai, China, Sep. 2020.

[19] Tsang, L., C. H. Chan, and H. Sangani, "Banded matrix iterative approach to Monte-Carlo simulations of scattering of waves by large-scale random rough surface problems: TM case," *Electronics Letters*, Vol. 29, No. 2, 166–167, 1993.

[20] Tsang, L., C. H. Chan, H. Sangani, A. Ishimaru, and P. Phu, "A banded matrix iterative approach to Monte Carlo simulations of large-scale random rough surface scattering: TE case," *Journal of Electromagnetic Waves and Applications*, Vol. 7, No. 9, 1185–1200, 1993.

[21] Tsang, L., C. H. Chan, K. Pak, and H. Sangani, "Monte-Carlo simulations of large-scale problems of random rough surface scattering and applications to grazing incidence with the BMIA/canonical grid method," *IEEE Transactions on Antennas and Propagation*, Vol. 43, No. 8, 851–859, 1995.

[22] Lucente, E., A. Monorchio, and R. Mittra, "An iteration-free MoM approach based on excitation independent characteristic basis functions for solving large multiscale electromagnetic scattering problems," *IEEE Transactions on Antennas and Propagation*, Vol. 56, No. 4, 999–1007, 2008.

[23] Elfouhaily, T., B. Chapron, K. Katsaros, and D. Vandemark, "A unified directional spectrum for long and short wind-driven waves," *Journal of Geophysical Research: Oceans*, Vol. 102, No. C7, 15 781–15 796, 1997.

[24] Thorsos, E. I., "The validity of the kirchhoff approximation for rough surface scattering using a Gaussian roughness spectrum," *The Journal of the Acoustical Society of America*, Vol. 83, No. 1, 78–92, 1988.

[25] Abromowitz, M. and I. A. Stegun, *Handbook of Mathematical Functions*, Dover publications, Inc., 1970.